Supplementary Materials of Microstructure-based modelling of snow mechanics: experimental evaluation on the cone penetration test

S1 Numerical sensitivity analysis

Prior computing DEM simulations on large scale numerical samples, a series of numerical sensitivity analysis are conducted in order to better understand the dependencies of the model on numerical parameters and choose optimised values. To limit the time allocated to this work, the sensitivity analyses are performed on a reduced numerical sample except for the numerical sample size sensitivity analysis. We choose a cubic numerical sample with a size of 8 mm and a rod radius 6 times smaller. The detailed investigations of sensitivity analysis are presented in the following sections.

S1.1 Grain shape representation

In the presented DEM simulations, a numerical grain is modelled with a collection of spheres capturing its arbitrary geometry. The downside of this grain shape representation is the potential involvement of a large amount of spheres and interactions resulting in time consuming computation. As we aim to run our DEM simulations on centimetres-sized numerical samples, involving thousands of grains, it is primordial to evaluate the dependence of the DEM model to the grain shape representation parameters to preserve a reliable mechanical behaviour along with a reasonable computing time. Especially, the mechanical behaviour accuracy is not strictly correlated to the number of spheres (Mede et al., 2018a). The two main shape parameters used in the grain shape representation, (1) the minimum sphere radius R and (2) the minimum sphere coverage S, have been varied. Their influence on the spheres number (consequently on the computation time), the grain number, interactions number, the volumetric accuracy and the mechanical response is investigated to establish the optimal shape parameters choice.

The sensitivity analysis has been repeated for the four snow types studied, i.e. RG, RGlr, DH and PP. Indeed, each snow type presents different grain characteristics and the optimised grain shape representation parameters may differ.

The grain shape representation accuracy is evaluated through the volumetric error E_V. It represents the error volume on the grain approximation and is computed as the volumetric difference between the effective original and the effective approximated image of the grain, divided by the total volume of the effective original grain image ($E_V = 0$ corresponds to a perfectly reconstructed grain). The medial axis method used for the grain approximation implies an underestimation of the grain volume (Coeurjolly and Montanvert, 2017, Mede et al., 2018). The global trend is that E_V decreases with the number of spheres increasing (Table S1 and Fig. S1). We also observe E_V increasing along with R and S. To evaluate the mechanical accuracy of the DEM simulations, the mechanical error E_M is computed, with the definition presented in Mede et al., 2018, as the normalised root mean square error of the force profile obtained relatively to a reference simulation. The reference simulation is defined as the R – S combination values providing the lowest E_V. The E_M is computed for force profile averaged

over a rolling window $\Delta z = 3$ mm (Table S1 and Fig. S1). It translates the likeliness of the force profile to the reference at the macroscale. The general trend observed is an increase of E_M with the E_V. However, we notice that relatively low E_M and low E_V can be reached for a moderate number of spheres (Table S1 and Fig. S1).

Sample	R	S	Number of spheres	Number of grains	Number of initial cohesive interactions between grains	E_V (%)	E_M (%)
RG	2	0.2	695380	8362	14839	10.0	0.0
	2	0.3	478330	8362	14839	14.6	19.8
	2	0.5	298981	8362	14839	22.6	48.3
	2	0.8	199996	8362	14839	35.2	71.6
	3	0.2	487094	8186	14642	14.2	36.7
	3	0.3	340295	8186	14642	17.7	56.4
	3	0.5	212439	8186	14642	24.9	71.7
	5	0.2	153208	6156	10501	41.1	6.9
	5	0.3	112139	6156	10501	42.9	13.8
	5	0.5	74243	6156	10501	46.6	23.6
RGlr	3	0.2	148078	2065	5111	9.2	0.0
	3	0.3	105859	2065	5111	13.1	31.4
	3	0.5	69365	2065	5111	21.3	5.9
	5	0.2	89053	1964	4963	11.1	20.4
	5	0.3	61251	1964	4963	14.9	18.0
	5	0.5	38256	1964	4963	22.5	38.6
	8	0.2	47924	1695	4363	18.2	44.3
DH	2	0.2	519856	3109	6144	7.8	0.0
	2	0.3	360490	3109	6144	11.6	5.6
	2	0.5	227247	3109	6144	19.5	51.3
	2	0.8	154331	3109	6144	32.9	10.6
	3	0.2	386882	3056	6085	10.2	5.6
	3	0.3	271824	3056	6085	13.6	19.4
	3	0.5	172874	3056	6085	20.8	31.5
	5	0.2	162919	67882	5147	24.9	12.7
	5	0.3	116547	2527	5147	27.4	25.8
	5	0.5	76067	2527	5147	32.6	18.9
PP	2	0.1	851438	19832	26217	17.4	0.0
	2	0.2	590590	19832	26217	20.3	1.8
	2	0.3	448132	19832	26217	24.4	8.3
	2	0.5	306191	19832	26217	32.0	9.6
	2	0.8	207615	19828	26212	44.0	22.3

Table S1 : Sum up of all the grain shape representation parameters. The chosen reference parameters display $E_M = 0$.

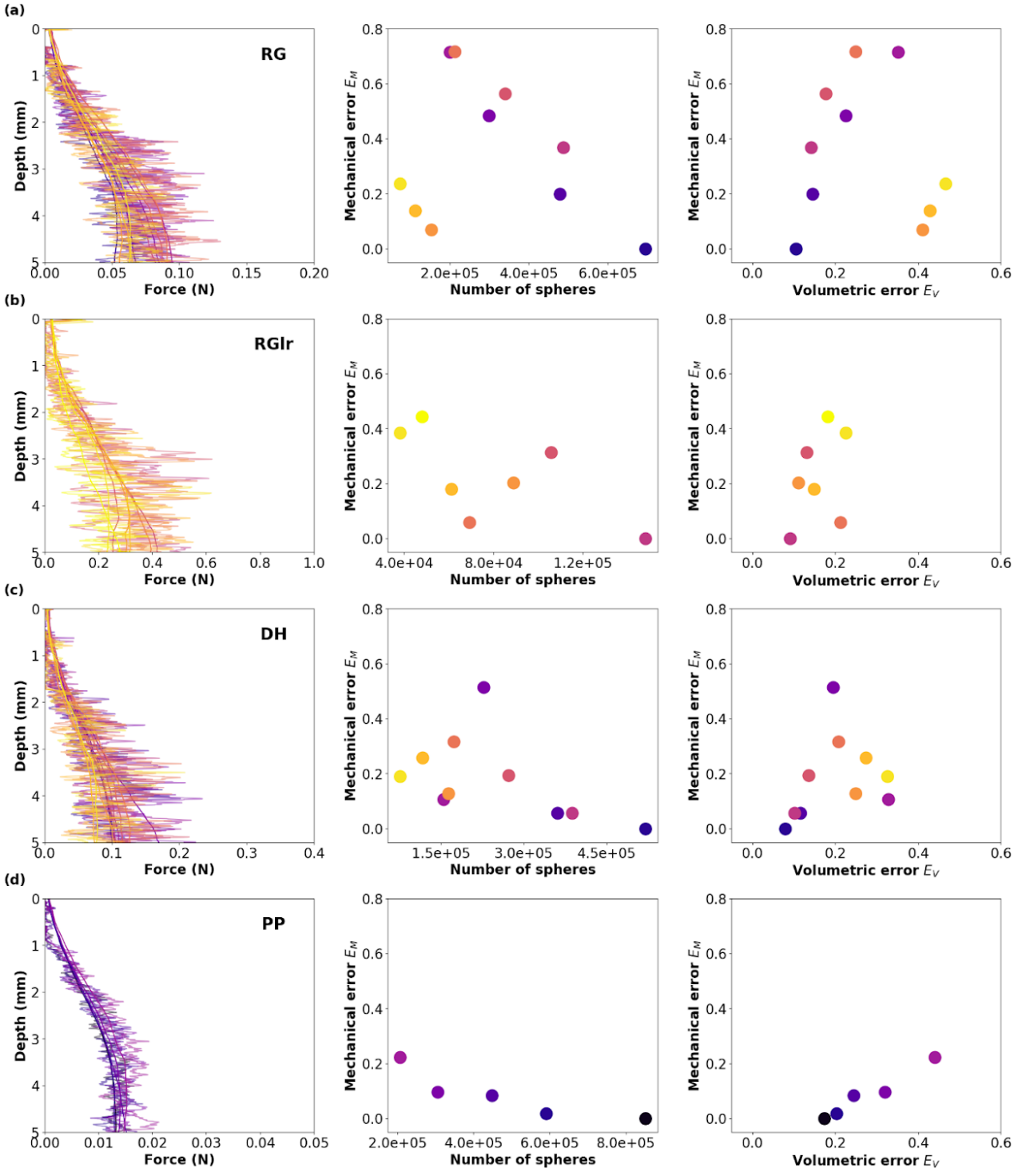
(a)
RG
Depth (mm)
Force (N)
Mechanical error E_M
Number of spheres
Volumetric error E_V
(b)
RGlr
(c)
DH
(d)
PP
R = 2.0 - S = 0.1
R = 2.0 - S = 0.2
R = 2.0 - S = 0.3
R = 2.0 - S = 0.5
R = 2.0 - S = 0.8
R = 3.0 - S = 0.2
R = 3.0 - S = 0.3
R = 3.0 - S = 0.5
R = 5.0 - S = 0.2
R = 5.0 - S = 0.3
R = 5.0 - S = 0.5
R = 8.0 - S = 0.2

Figure S1: Grain shape representation sensitivity analysis performed for the different types of snow studied: RG, RGlr, DH and PP. The minimum sphere radius R and the minimum sphere coverage S have been varied influencing the spheres number. (a) Force profiles (light coloured lines) with superposed smooth profile (force averaged over a rolling window of 3 mm). (b) Evolution of the volumetric error E_V with respect to the number of spheres for each R – S combination. (c) Volumetric error E_V vs Mechanical error E_M. The reference run to compute E_M corresponds to the numerical sample with the maximum of spheres.

In order to choose the respective shape parameters for each snow type, we selected below an E_M threshold of 20% the numerical sample with a reduced spheres number allowing reasonable computation time. This might imply selecting a numerical sample with a relative high E_V.

S1.2 Numerical sample size

Numerical sample size plays a strong role in the numerical computation time. Larger numerical sample size involves larger amounts of grains and a larger amount of spheres and interactions. The CPT configuration allows some freedom to adapt the size of the numerical sample without introducing border effects. To evaluate the numerical sample size sensitivity, we compared the force profiles obtained for different numerical sample sizes to the force profile obtained for a reference simulation computed with the largest possible numerical sample size along the x and y axis (14.1 mm border size) by calculating the mechanical error E_M (Sect. S1.1). The tip radius is set to 2.5 mm in accordance with the SMP tip radius (Sect. 2.1.3). The depth of the numerical sample is set at a constant value of 12 mm. The analysis is performed only for the snow sample type RGlr as it displays the largest grain size (Table 1), so is the most likely to be affected by border effects. We assume the results can be applied to the other snow samples with smaller grain sizes.

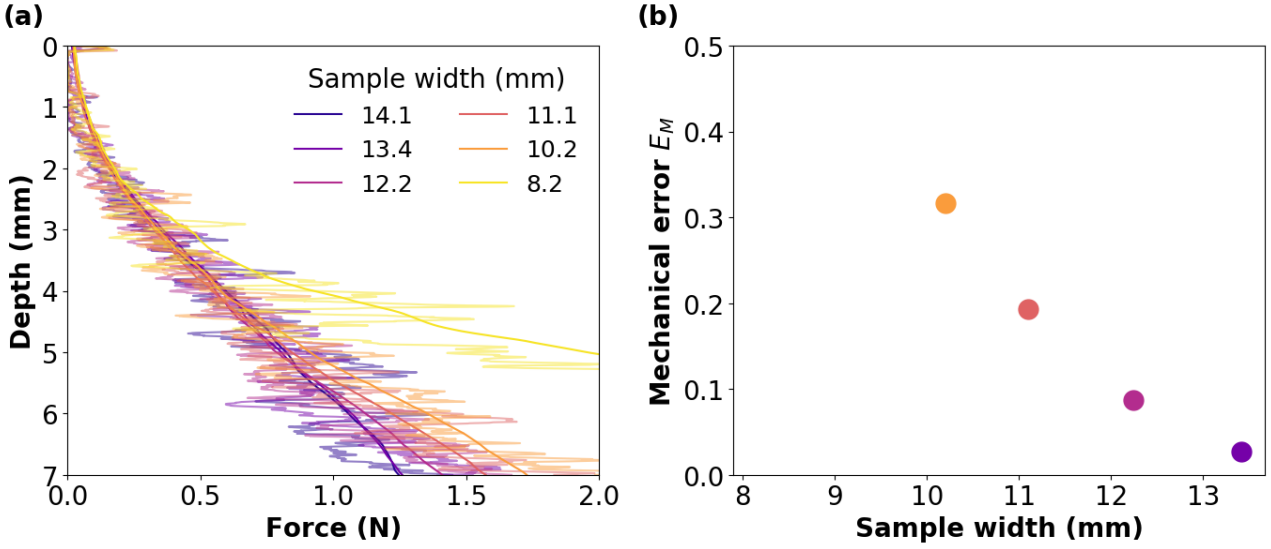

Figure S2: Sensitivity analysis on the numerical sample size. (a) Force profiles (light coloured lines) with superposed smooth profile (force averaged over a rolling window of 3 mm). (b) Mechanical error E_M in function of the numerical sample width. The reference

force profile has been obtained with a size of 14.1 mm. The point for a sample width of 8.2 mm is out of range in the panel (b). The results are presented for the RGlr sample.

We observed numerical sample sizes up to 12 mm guarantee the consistency of the mechanical behaviour with an E_M below 20% (Fig. S2). We chose a numerical sample size of 12.4 mm to perform our numerical simulations.

S1.3 Motion equation parameters

Sensitivity analyses are performed on parameters dedicated to numerical stability.

The time step can be modified by artificially adjusting the grain mass with a mass factor (Hagenmuller et al., 2015) (Eq. (6), Sect. 2.2.3). The results show mass factors up to 1 x 10^4 provide consistent results with results obtained with a mass factor of 1 (Fig. S3). We set the mass factor to 1 x 10^2 for all the presented numerical simulation results.

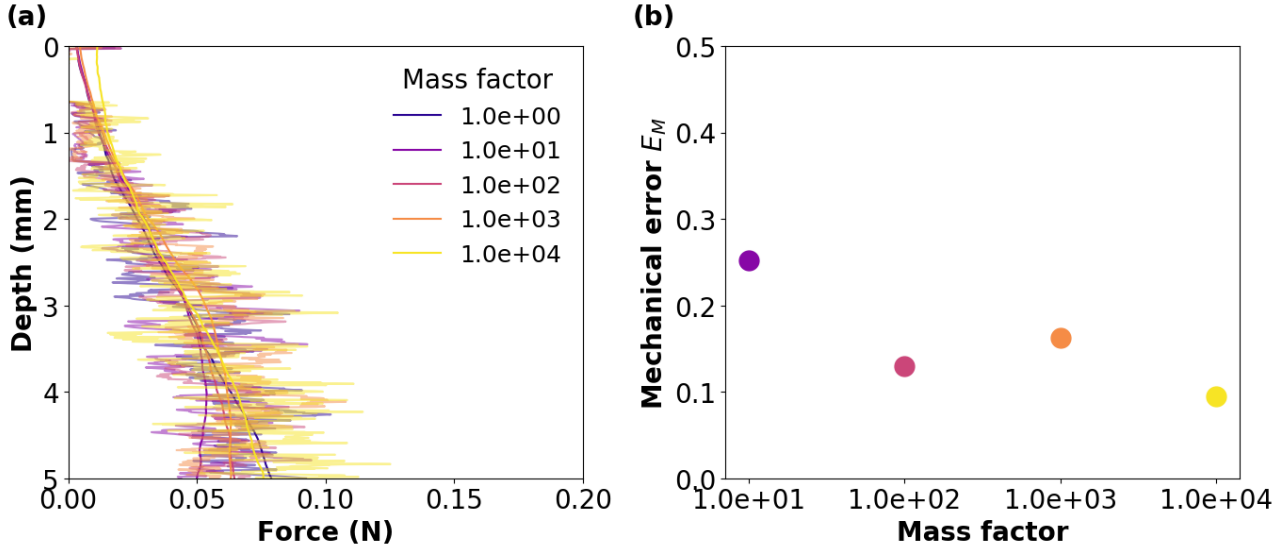

Figure S3: Sensitivity of the mechanical behaviour to the mass factor. (a) Force profiles (light coloured lines) with superposed smooth profile (force averaged over a rolling window of 3 mm). (b) Mechanical error E_M in function of the numerical sample size. The reference force profile has been obtained with a mass factor of 1. The results are presented for the RG sample.

The Cundall's non viscous damping coefficient is applied to prevent numerical oscillation. The sensitivity analysis results presented in Fig. S4, shows this parameter does not display a strong influence on the resulting force profiles. A value of 0.05 is chosen.

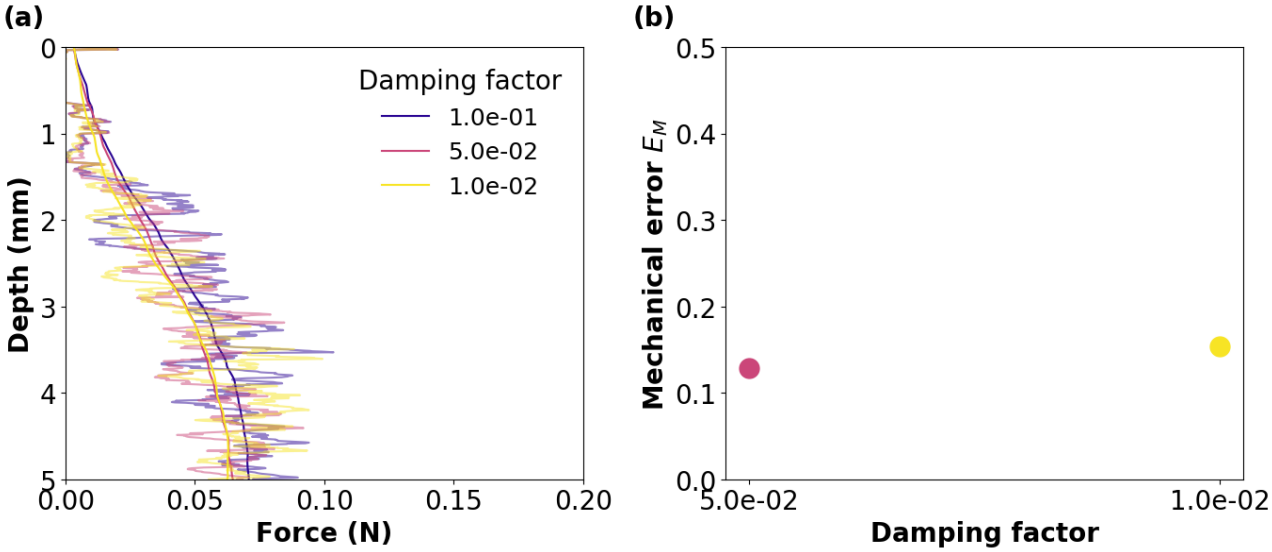

Figure S4: Sensitivity of the mechanical behaviour to the Cundall's non viscous damping coefficient. (a) Force profiles (light coloured lines) with superposed smooth profile (force averaged over a rolling window of 3 mm). (b) Mechanical error E_M in function of the damping factor. The reference force profile has obtained a damping factor of 0.1.

S1.4 Grain rigidity

In order to ensure the rigid (unbreakable) grain assumption in the elastic-brittle regime the overlap between spheres of grains in contact must remain under a few percent of the sphere's radius. The grain stiffness is dependent on Young's modulus which is a parameter that has been varied in our study. To verify the grain rigidity assumption is valid for all the values tested, a sensitivity analysis has been conducted. Figure S5 shows that for Young's modulus values ($E = 1 \times 10^8$-1×10^{10} Pa) chosen for our study, the relative overlap remains negligible (under 1%) ensuring the grain rigidity. For lower Young's modulus ($E \leq 1 \times 10^7$ Pa) relative overlap increases to several percent that cannot guarantee the grain rigidity.

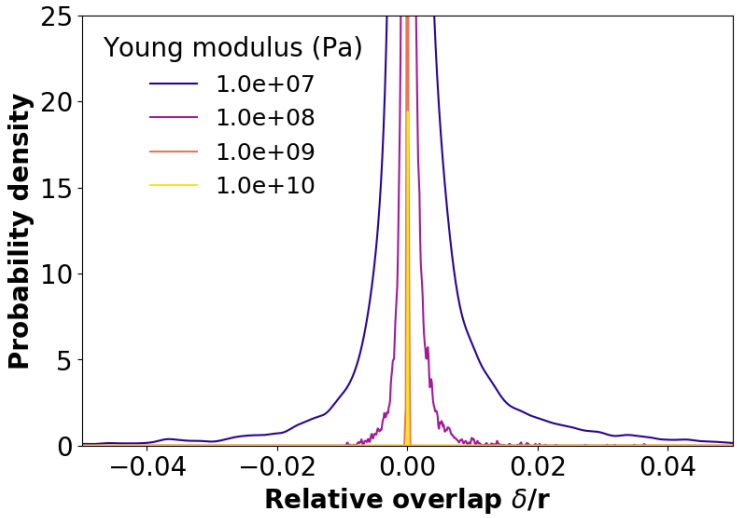

Figure S5: Occurrence distribution of the relative grains overlap at a tip penetrating depth of 3 mm for different Young's modulus E (Pa). The results are presented for the RG sample.

S2 Additional results

S2.1 Cone Penetration Tests on numerical samples with DEM

S2.1.1 RGlr sample

The force of the RGlr sample increases with depth along with fluctuations amplitude (Fig. S6 (a)). The macroscopic force follows a 'S' shape evolution with a first stage characterised by a force increase with a shallow slope and larger fluctuation amplitude (around 2.5 mm depth), then a second stage with a slope increase (between ~2.5 and ~8 mm depth) and finally a third stage with a slope decrease until a nearly constant macroscopic force value.

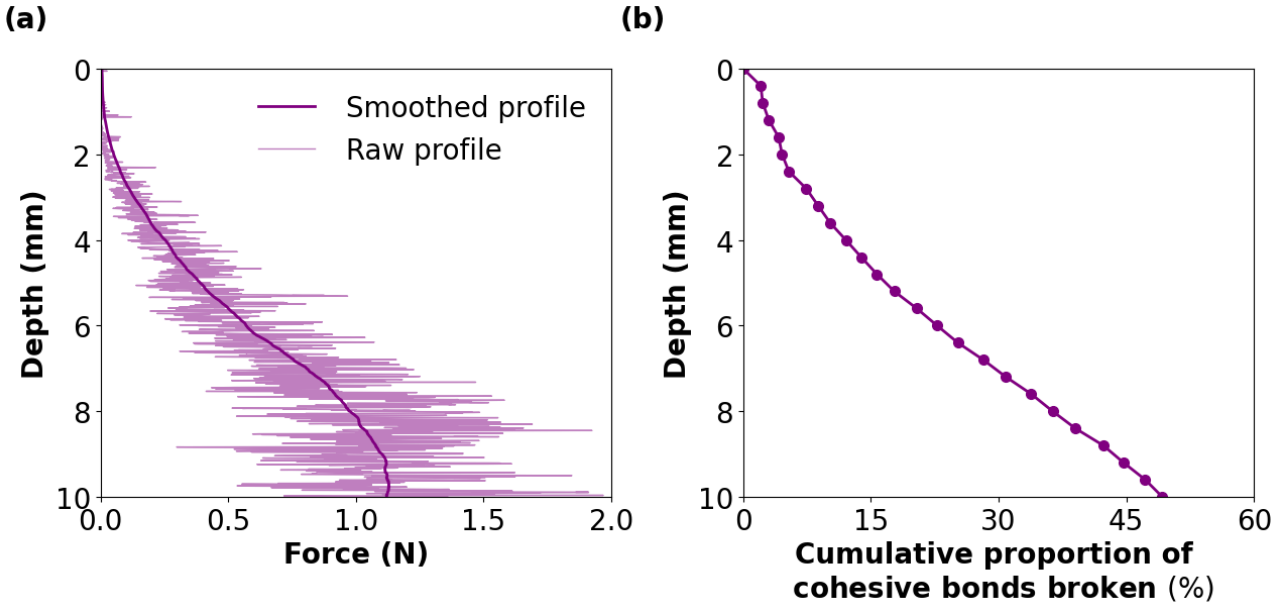

Figure S6: (a) Force as function of depth (light line) obtained for the RGlr sample. The superposed smoothed profile (bold line) corresponds to the average force value over a rolling window of 3 mm. (b) Cumulative number of cohesive bonds as function of tip penetration depth. Results are obtained with the mechanical parameters given in Table 3.

The number of bonds failure as a function of depth globally evolves at a constant rate (Fig. S6 (b)). For the RG sample, about 70% of the cohesive interactions broke over 10 mm during the CPT leading to an average rate of ~1000 bonds failure mm^{-1}. We notice a slight increase of bond failure slope around 2.5 mm tip depth coinciding with the depth of slope and fluctuation amplitude change between the first and second stage observed in the force signal (Fig. S6 (a)). No slope change is observed for the transition between the second and the third stages observed in the force profile where a steady state of the macroscopic force is reached. In this case, no change in the force fluctuation amplitude is observed.

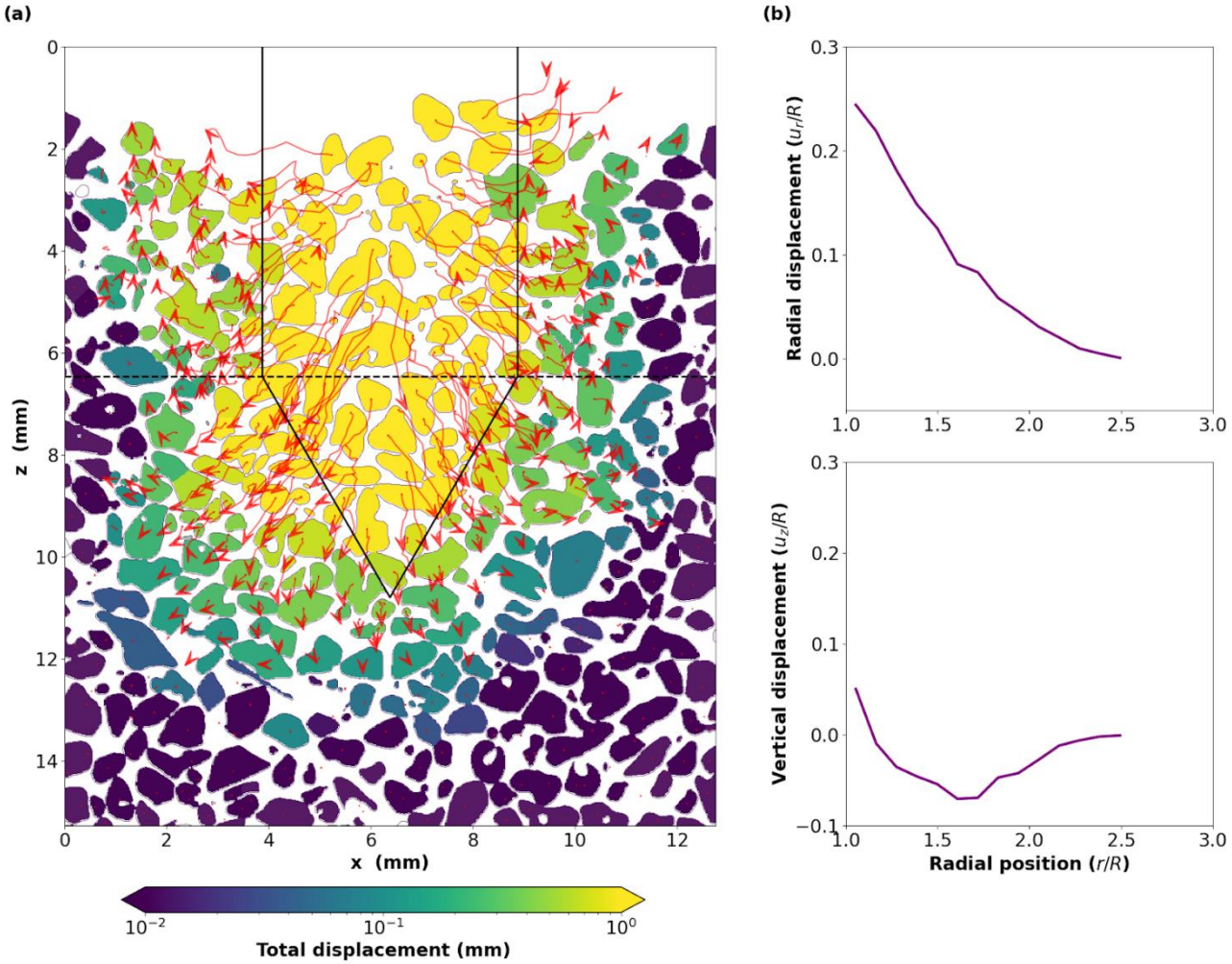

Figure S7: (a) Total grain displacement maps of the RGlr sample. The red arrows indicate the grain path while the tip is penetrating (sampling = 0.4 mm). (b) Radial (upper panel) and vertical (lower panel) displacement profiles for the RGlr sample. By convention, downward movement corresponds to positive value and upward movement corresponds to negative values. Results are obtained with the mechanical parameters given in Table 3.

For the RGlr sample, the displacement field presents complex characteristics (Fig. S7 (a)). The grains are mainly pushed downward and from each side of the tip. Grains located on the middle of the tip path display a quasi-straight path and the grain pushed aside displays a curved trajectory. Close to the surface, the curved trajectory is oriented upwards. The magnitude of the downward component of the curved trajectory is increasing with depth. Below the cone top, the grains trajectories present predominantly a quasi linear trend, from a mainly radial orientation at the cone top to a mainly downward orientation at the cone tip. The trajectory becomes more radial as the grains are located away from the tip.

This curved trajectory oriented upward in the area situated between the sample surface and the cone top is transcribed in the average vertical displacement profiles (Fig. S7 (b)). We observe a transition from downward movement close to the tip to an increase of the upward influence away until the movement reaches zero around 2.5R. We notice that the averaged vertical

displacement is almost zero, the upward movements are compensated by downward movements. The radial trajectory follows a quasi linear trend with large grain displacement and reaching 0 around 2.5R.

S2.1.2 DH sample

The force of the DH sample increases with depth along with fluctuations amplitude (Fig. S8 (a)). The macroscopic force follows a 'S' shape evolution with a first stage characterised by a force increase with a shallow slope and larger fluctuation amplitude (around 2.0 mm), then a second stage with a slope increase (between ~2.0 and ~8 mm depth) and finally a third stage with a slope decrease until a nearly constant macroscopic force value.

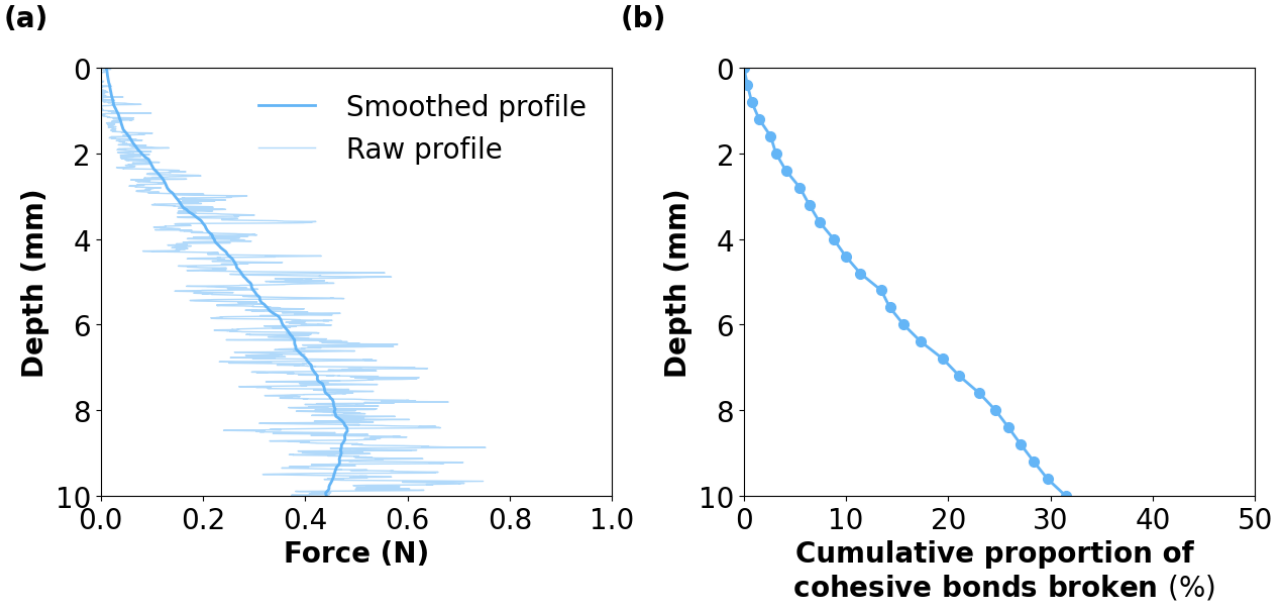

Figure S8 : (a) Force as function of depth (light line) obtained for the DH sample. The superposed smoothed profile (bold line) corresponds to the average force value over a rolling window of 3 mm. (b) Cumulative number of cohesive bonds as function of tip penetration depth. Results are obtained with the mechanical parameters given in Table 3.

The number of bonds failure as a function of depth globally evolves at a constant rate (Fig. S8 (b)). For the DH sample, about 32% of the cohesive interactions broke over 10 mm during the CPT leading to an average rate of ~690 bonds failure mm^{-1}. No clear slope change is observed in the interaction profile.

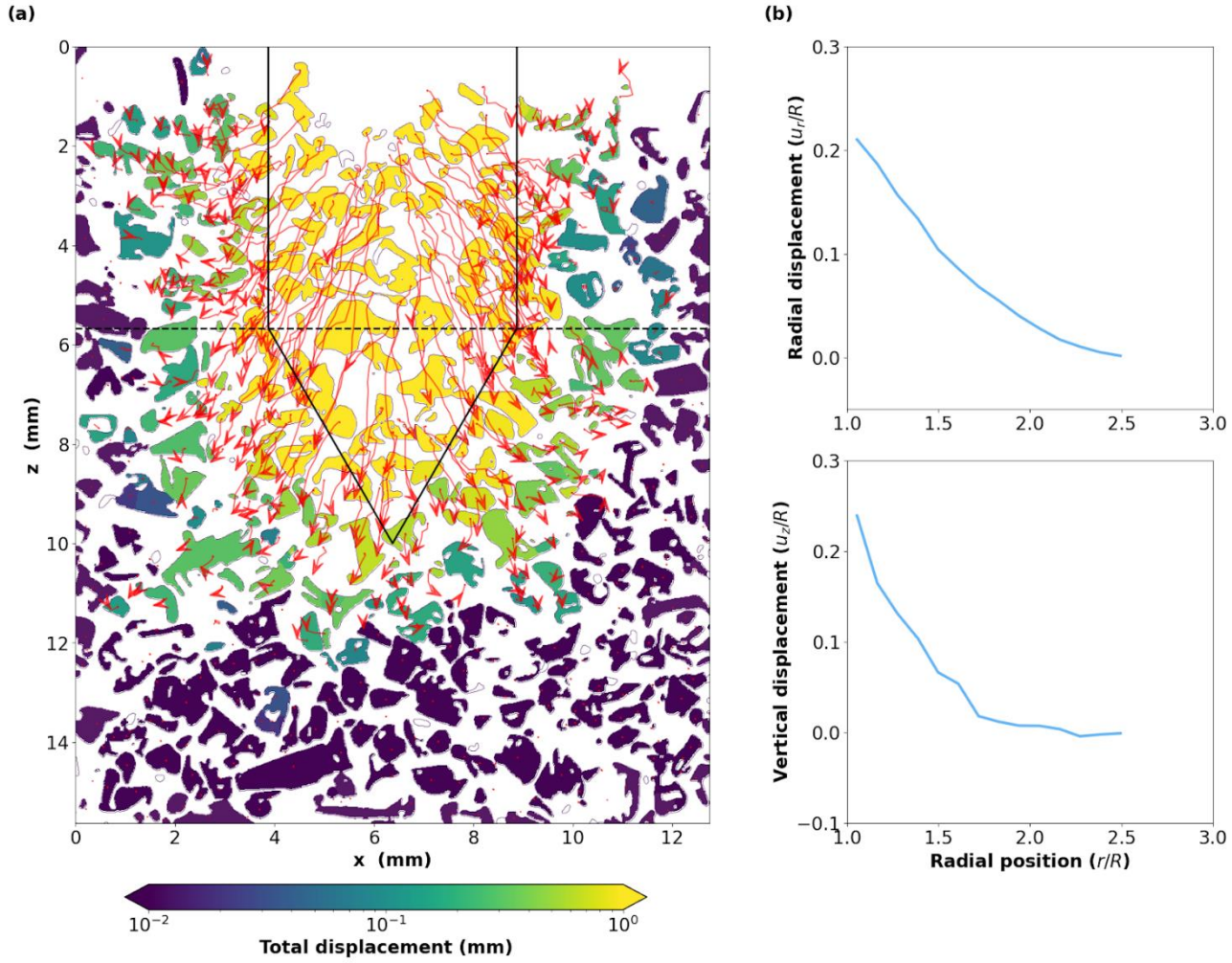

Figure S9 : (a) Total grain displacement maps of the DH sample. The red arrows indicate the grain path while the tip is penetrating (sampling = 0.4 mm). (b) Radial (upper panel) and vertical (lower panel) displacement profiles for the DH sample. By convention, downward movement corresponds to positive value and upward movement corresponds to negative values. Results are obtained with the mechanical parameters given in Table 3.

Figure S9a shows the total displacement of the grains and their respective trajectories for the DH sample. The largest displacements (up to several mm) are observed for grains initially located on the trajectory of the tip, while around the tip the displacements are < 1 mm and are mainly localised close to the tip. Grain trajectories indicate that grains are pushed downward from each side of the tip. The grains initially located on the middle of the tip path display a quasi-straight vertical trajectory. The trajectories become more radial away from the tip medial axis, with the grains being also pushed aside. The grain trajectories are predominantly linear, with an almost radial orientation at the cone top and a more vertical orientation near the tip. Both radial and vertical displacement profiles show a pronounced decreasing trend, and reach zero at a radial position of

about 2.5R and 2.3R respectively (Fig. S9 (b)). The vertical profile attests of a dominant downward movement of the grains close to the tip.

S2.1.3 PP sample

The force of the PP sample increases with depth along with fluctuations amplitude (Fig. S10 (a)). The macroscopic force follows a 'S' shape evolution with a first stage characterised by a force increase with a shallow slope and larger fluctuation amplitude (around 2.0 mm depth), then a second stage with a slope increase (between ~2.0 and ~5 mm) and finally a third stage with a slope decrease until a nearly constant macroscopic force value.

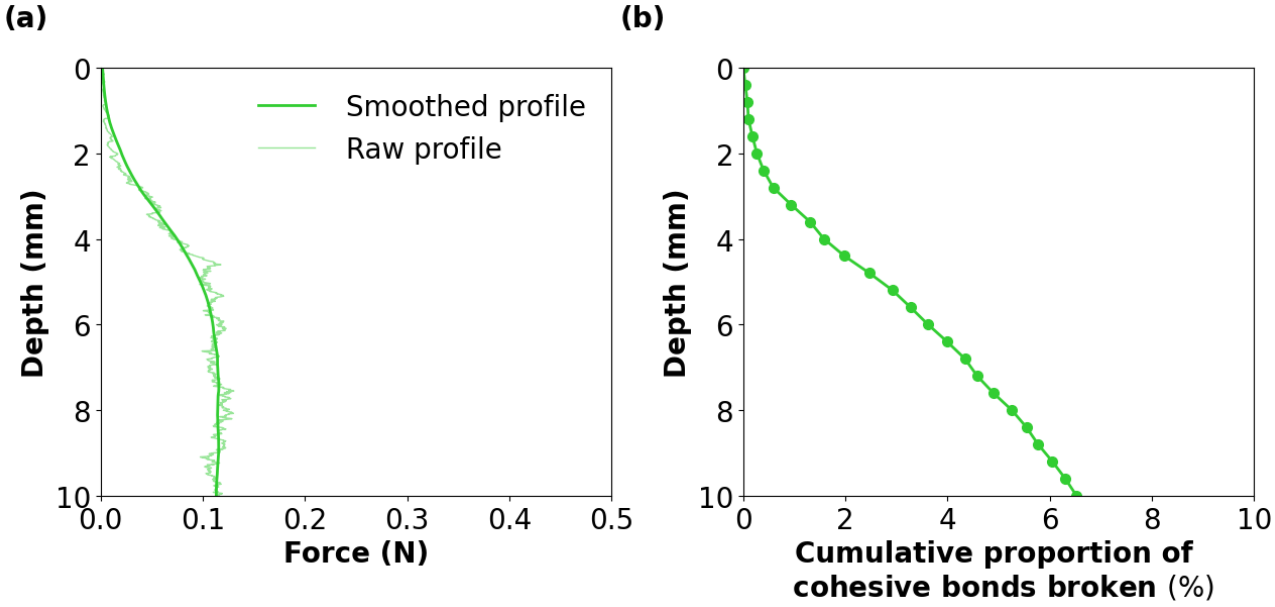

Figure S10: (a) Force as function of depth (light line) obtained for the PP sample. The superposed smoothed profile (bold line) corresponds to the average force value over a rolling window of 3 mm. (b) Cumulative number of cohesive bonds as function of tip penetration depth. Results are obtained with the mechanical parameters given in Table 3.

The number of bonds failure as a function of depth globally evolves at a constant rate (Fig. S10 (b)). For the PP sample, about 7% of the cohesive interactions broke over 10 mm during the CPT leading to an average rate of ~1090 bonds failure mm^{-1}. We notice a slight increase of bond failure slope around 2.5 mm tip depth that may be related to the fluctuation amplitude change between the first and second stage observed in the force signal (Fig. S10 (a)). No clear slope change is observed for the transition between the second and the third stages observed in the force profile where a steady state of the macroscopic force is reached.

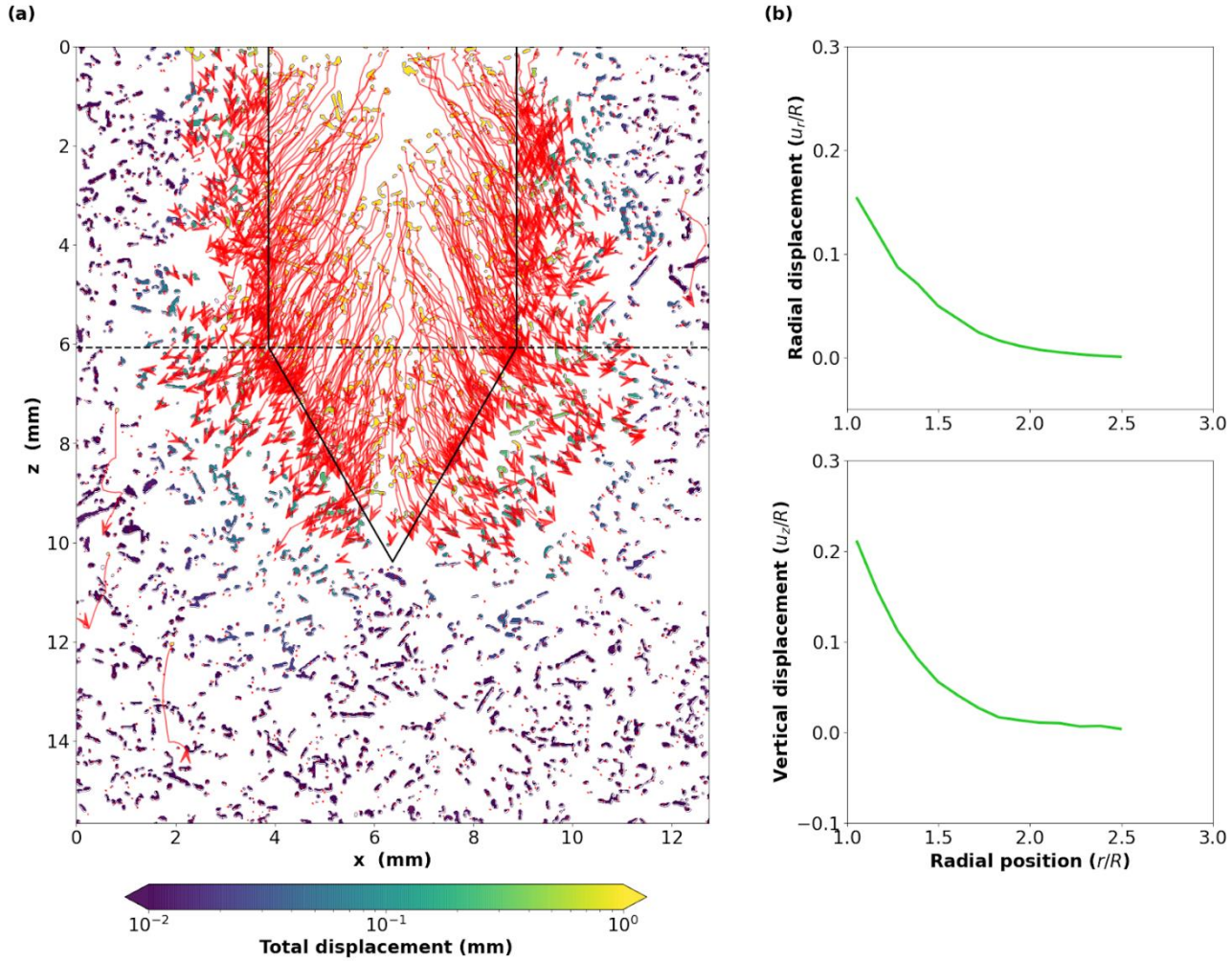

Figure S11 : (a) Total grain displacement maps of the PP sample. The red arrows indicate the grain path while the tip is penetrating (sampling = 0.4 mm). (b) Radial (upper panel) and vertical (lower panel) displacement profiles for the PP sample. By convention, downward movement corresponds to positive value and upward movement corresponds to negative values. Results are obtained with the mechanical parameters given in Table 3.

Figure S11a shows the total displacement of the grains and their respective trajectories for the PP sample. The largest displacements (up to several mm) are observed for grains initially located on the trajectory of the tip, while around the tip the displacements are < 1 mm and are mainly localised close to the tip. Grain trajectories indicate that grains are pushed downward from each side of the tip. The grains initially located on the middle of the tip path display a quasi-straight vertical trajectory. The trajectories become more radial away from the tip medial axis, with the grains being also pushed aside. The grain trajectories are predominantly linear, with a rather vertical orientation at the cone top and a more radial orientation near the tip. Both radial and vertical displacement profiles show a pronounced decreasing and concave trend, and reach zero at a radial

position of about 2.3R (Fig. S11 (b)). The vertical profile attests of a dominant downward movement of the grains close to the tip.

S2.2 Mechanical parameters sensitivity analysis

In this section, the figures obtained for the mechanical parameters sensitivity analysis are presented respectively to each sample. The description and interpretation of the plots can be found in the core of the article (Sect. 3.2 and 3.3) .

S2.2.1 RG sample

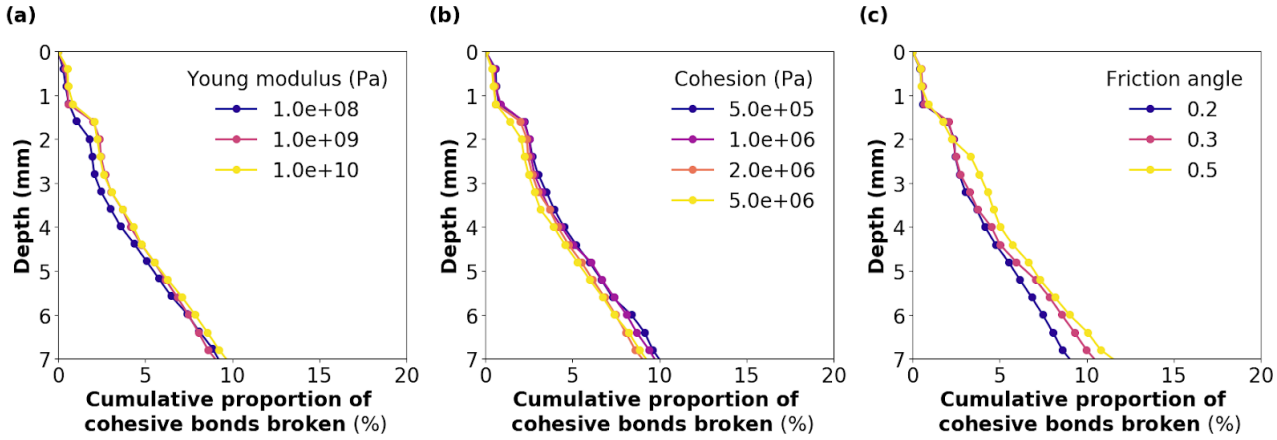

Figure S12: Influence of mechanical parameters on the cumulative number of cohesive bonds as function of tip penetration depth obtained with DEM numerical simulations of CPT. The sensitivity analysis has been performed on (a) Young's modulus E (Pa) (C = 2.0 x 10^6 Pa and tan(φ) = 0.2), (b) the Cohesion C (Pa) (E = 1.0 x 10^9 Pa and tan(φ) = 0.2) and (c) the Friction angle tan(φ) (E = 1.0 x 10^9 Pa and C = 2.0 x 10^6 Pa).

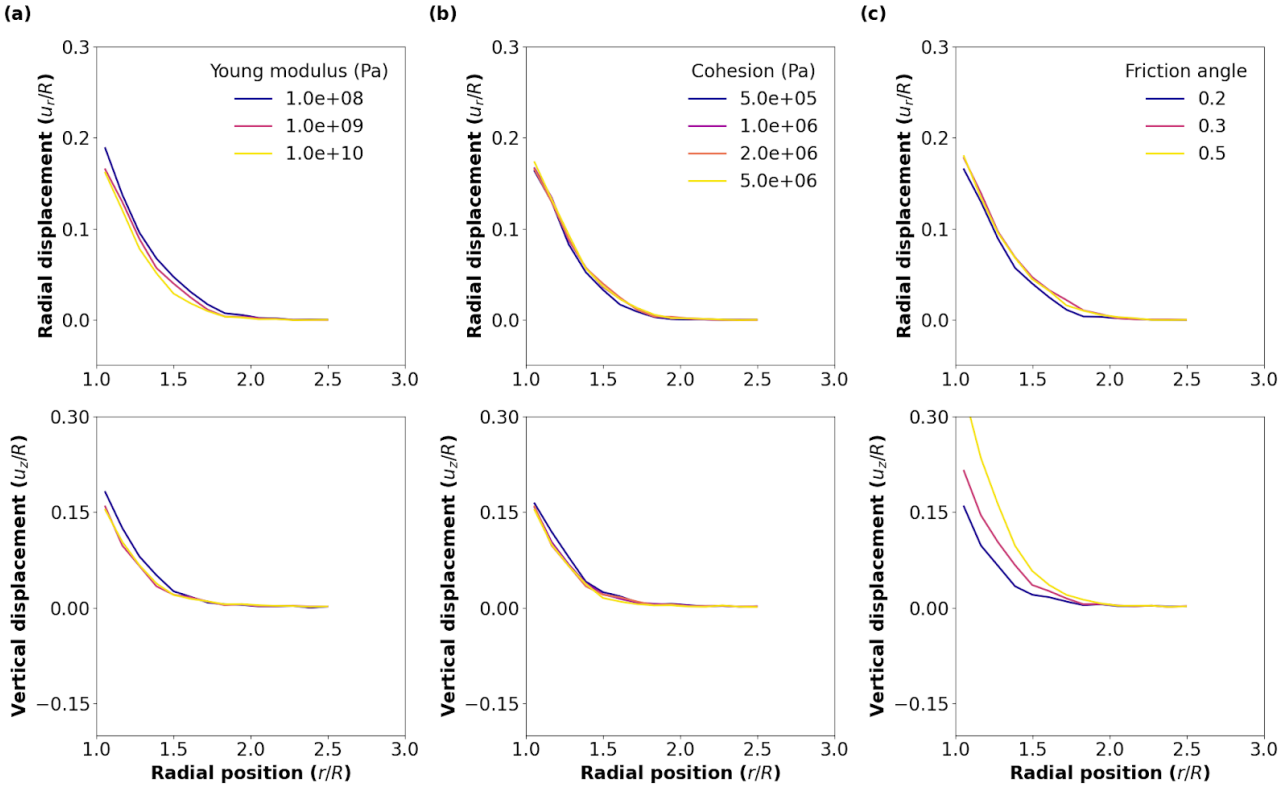

Figure S13 : Influence of mechanical parameters on the radial (top) and vertical (bottom) displacement profile obtained with DEM numerical simulations of CPT. The sensitivity analysis has been performed on (a) Young's modulus E (Pa) (C = 2.0 x 10^6 Pa and tan(φ) = 0.2), (b) the Cohesion C (Pa) (E = 1.0 x 10^9 Pa and tan(φ) = 0.2) and (c) the Friction angle tan(φ) (E = 1.0 x 10^9 Pa and C = 2.0 x 10^6 Pa).

S2.2.2 RGlr sample

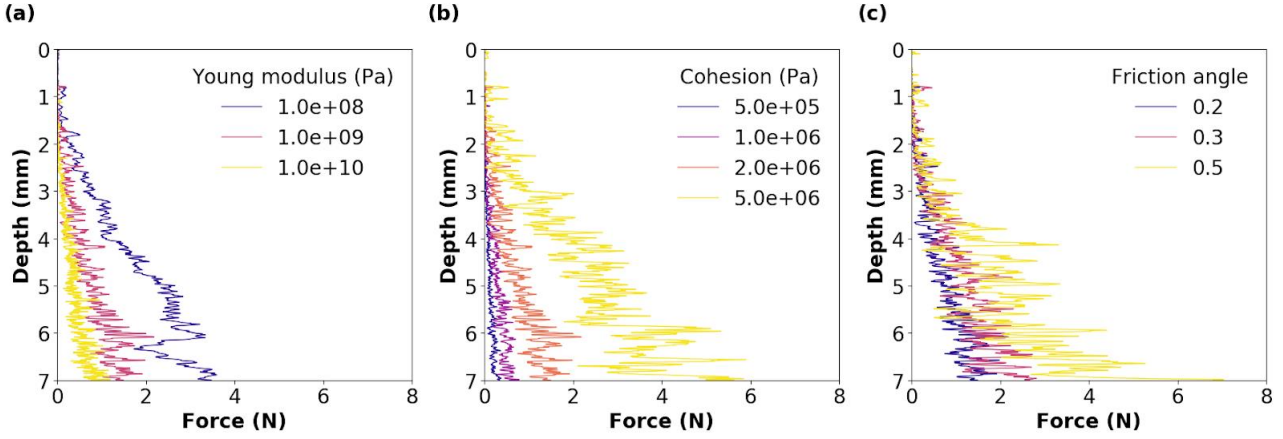

Figure S14*:* Influence of mechanical parameters on the force profile obtained with DEM numerical simulations of CPT. The sensitivity analysis has been performed on (a) Young's modulus E (Pa) (C = 2.0 x 10^6 Pa and tan(φ) = 0.2), (b) the Cohesion C (Pa) (E = 1.0 x 10^9 Pa and tan(φ) = 0.2) and (c) the Friction angle tan(φ) (E = 1.0 x 10^9 Pa and C = 2.0 x 10^6 Pa).

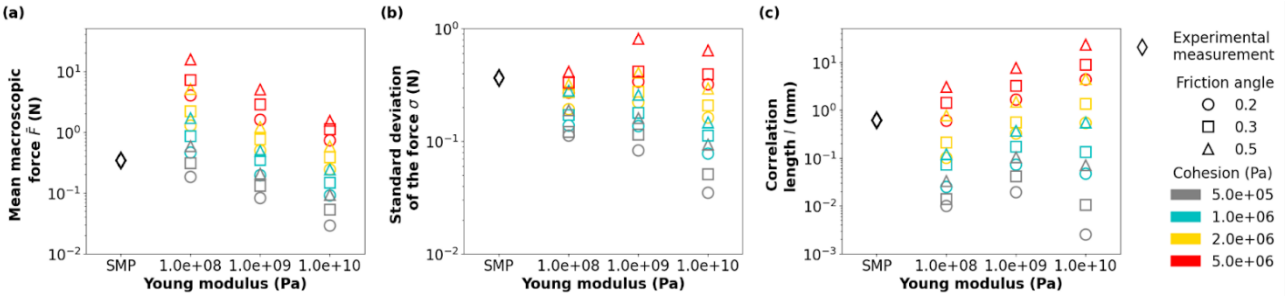

Figure S15*:* Evolution of statistical indicators as function of Young's modulus, cohesion and friction angle: (a) Mean macroscopic force, (b) standard deviation of the force, and (c) correlation length. The experimental results (black diamonds) have been added to the plots. Results presented here correspond to the RGlr sample.

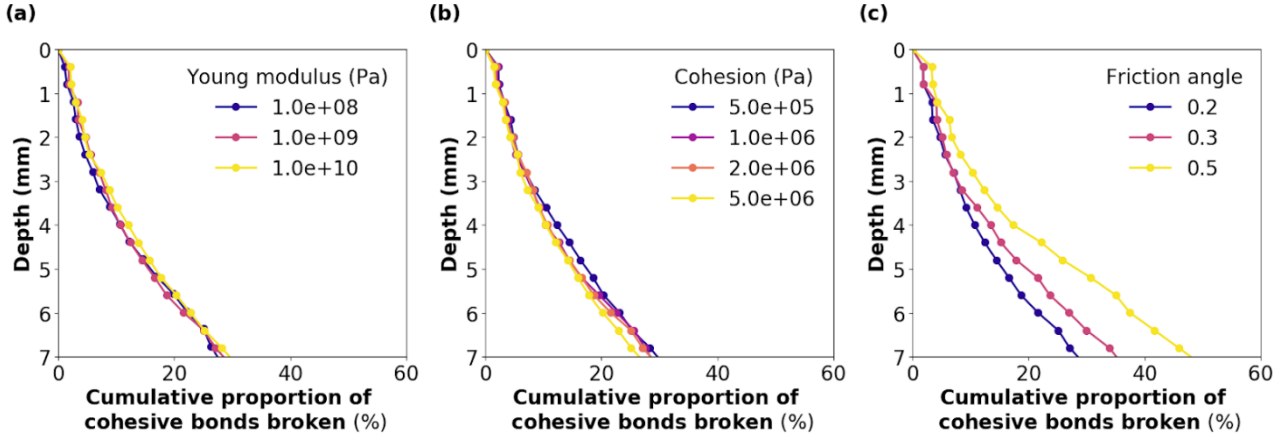

Figure S16: Influence of mechanical parameters on the cumulative number of cohesive bonds as function of tip penetration depth obtained with DEM numerical simulations of CPT. The sensitivity analysis has been performed on (a) Young's modulus E (Pa) (C = 2.0 x 10^6 Pa and tan(φ) = 0.2), (b) the Cohesion C (Pa) (E = 1.0 x 10^9 Pa and tan(φ) = 0.2) and (c) the Friction angle tan(φ) (E = 1.0 x 10^9 Pa and C = 2.0 x 10^6 Pa).

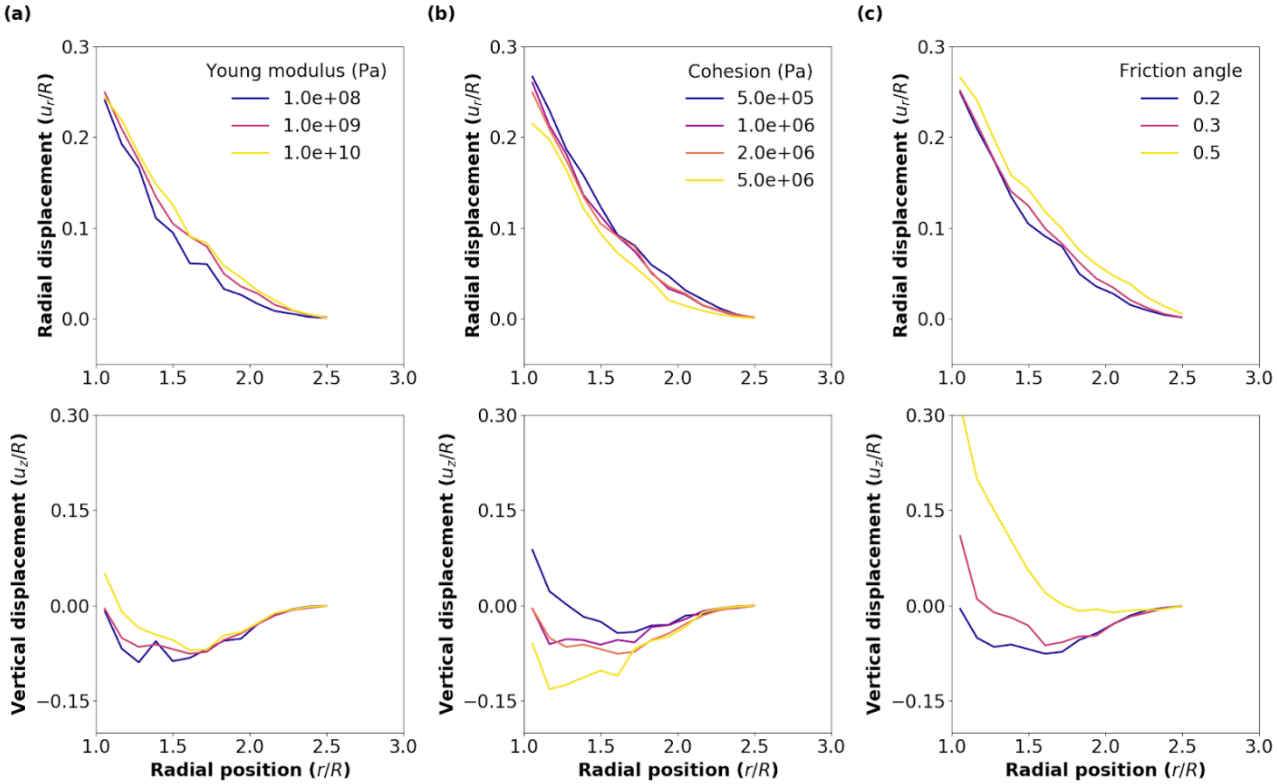

Figure S17: Influence of mechanical parameters on the radial (top) and vertical (bottom) displacement profile obtained with DEM numerical simulations of CPT. The sensitivity analysis has been performed on (a) Young's modulus E (Pa) (C = 2.0 x 10^6 Pa and tan(φ) = 0.2), (b) the Cohesion C (Pa) (E = 1.0 x 10^9 Pa and tan(φ) = 0.2) and (c) the Friction angle tan(φ) (E = 1.0 x 10^9 Pa and C = 2.0 x 10^6 Pa).

S2.2.3 DH sample

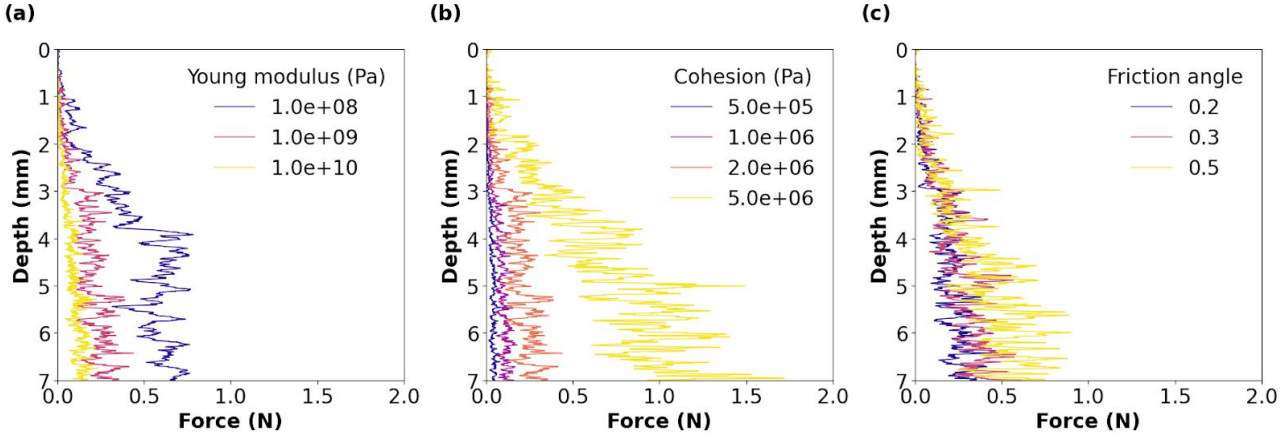

Figure S18: Influence of mechanical parameters on the force profile obtained with DEM numerical simulations of CPT. The sensitivity analysis has been performed on (a) Young's modulus E (Pa) (C = 2.0 x 10^6 Pa and tan(φ) = 0.2), (b) the Cohesion C (Pa) (E = 1.0 x 10^9 Pa and tan(φ) = 0.2) and (c) the Friction angle tan(φ) (E = 1.0 x 10^9 Pa and C = 2.0 x 10^6 Pa).

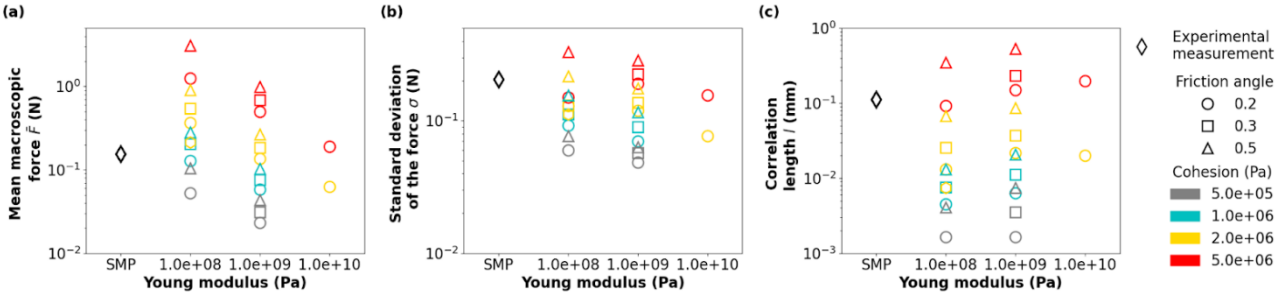

Figure S19: Evolution of statistical indicators as function of Young's modulus, cohesion and friction angle: (a) Mean macroscopic force, (b) standard deviation of the force, and (c) correlation length. The experimental results (black diamonds) have been added to the plots. Results presented here correspond to the DH sample.

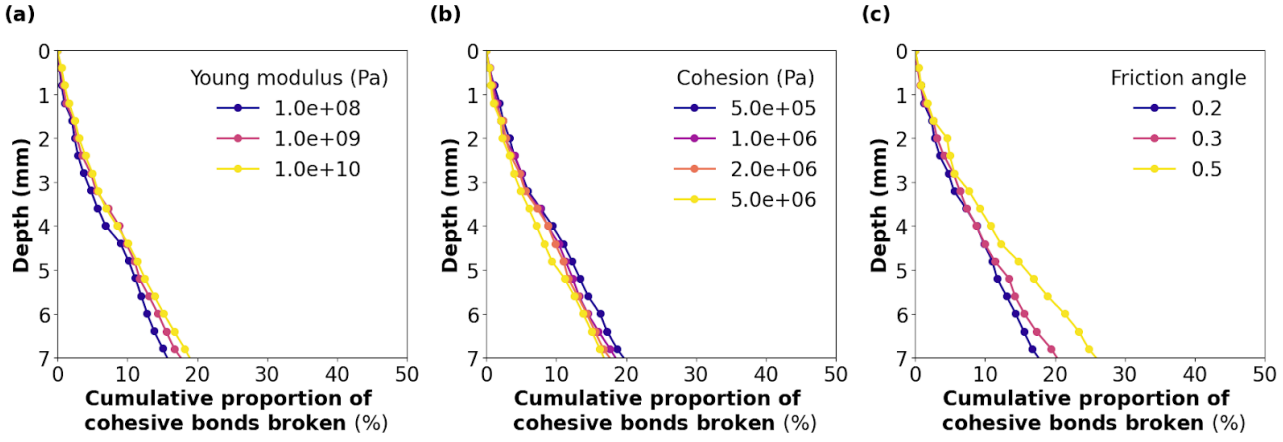

Figure S20: Influence of mechanical parameters on the cumulative number of cohesive bonds as function of tip penetration depth obtained with DEM numerical simulations of CPT. The sensitivity analysis has been performed on (a) Young's modulus E (Pa) (C = 2.0 x 10^6 Pa and tan(φ) = 0.2), (b) the Cohesion C (Pa) (E = 1.0 x 10^9 Pa and tan(φ) = 0.2) and (c) the Friction angle tan(φ) (E = 1.0 x 10^9 Pa and C = 2.0 x 10^6 Pa).

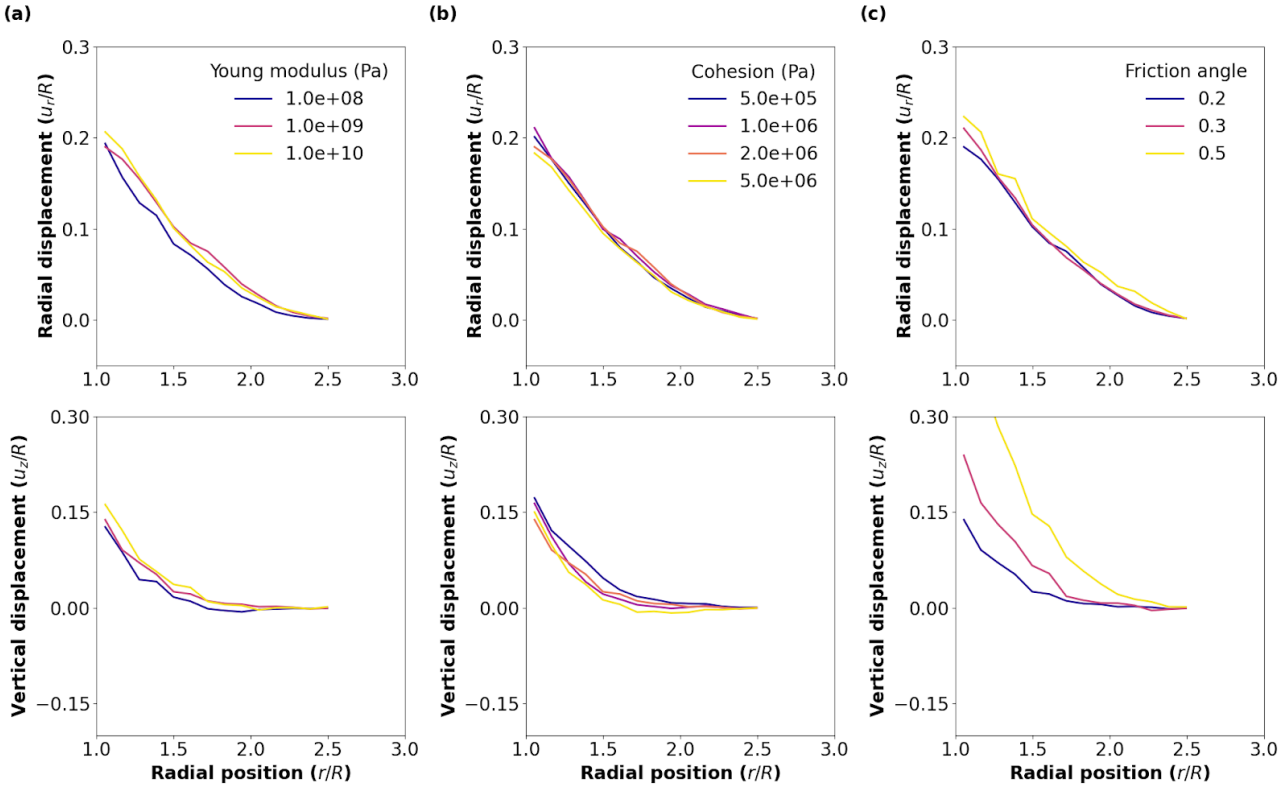

Figure S21: Influence of mechanical parameters on the radial (top) and vertical (bottom) displacement profile obtained with DEM numerical simulations of CPT. The sensitivity analysis has been performed on (a) Young's modulus E (Pa) (C = 2.0 x 10^6 Pa and tan(φ) = 0.2), (b) the Cohesion C (Pa) (E = 1.0 x 10^9 Pa and tan(φ) = 0.2) and (c) the Friction angle tan(φ) (E = 1.0 x 10^9 Pa and C = 2.0 x 10^6 Pa).

S2.2.4 PP sample

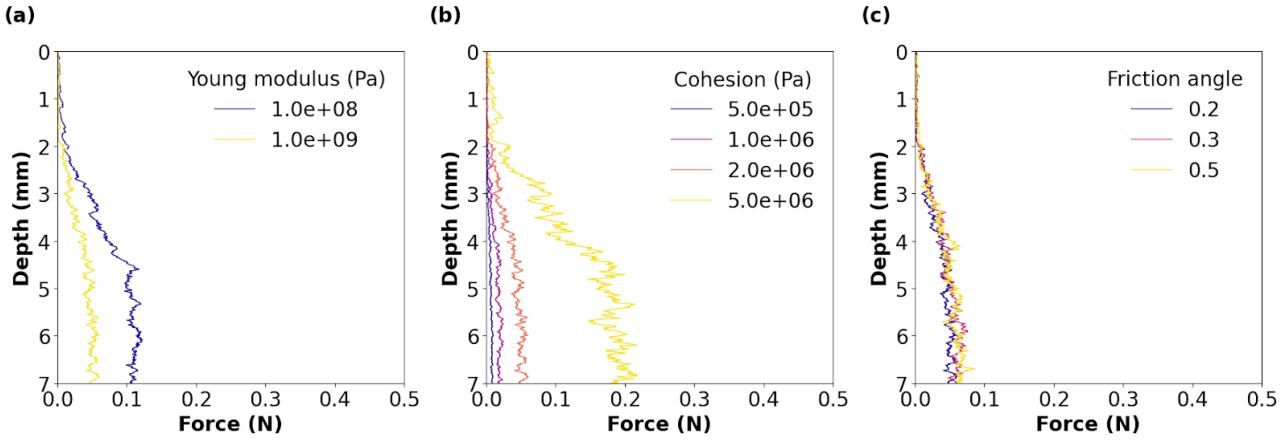

Figure S22: Influence of mechanical parameters on the force profile obtained with DEM numerical simulations of CPT. The sensitivity analysis has been performed on (a) Young's modulus E (Pa) (C = 1.0 x 10^6 Pa and tan(φ) = 0.2), (b) the Cohesion C (Pa) (E = 1.0 x 10^8 Pa and tan(φ) = 0.2) and (c) the Friction angle tan(φ) (E = 1.0 x 10^8 Pa and C = 1.0 x 10^6 Pa).

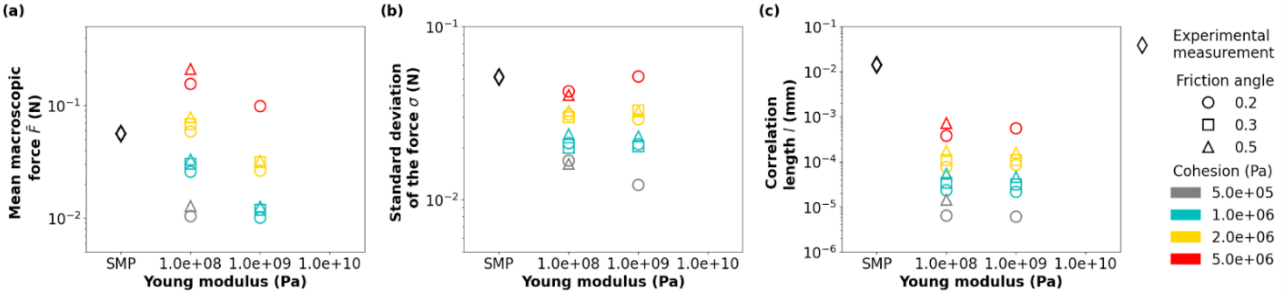

Figure S23: Evolution of statistical indicators as function of Young's modulus, cohesion and friction angle: (a) Mean macroscopic force, (b) standard deviation of the force, and (c) correlation length. The experimental results (black diamonds) have been added to the plots. Results presented here correspond to the PP sample.

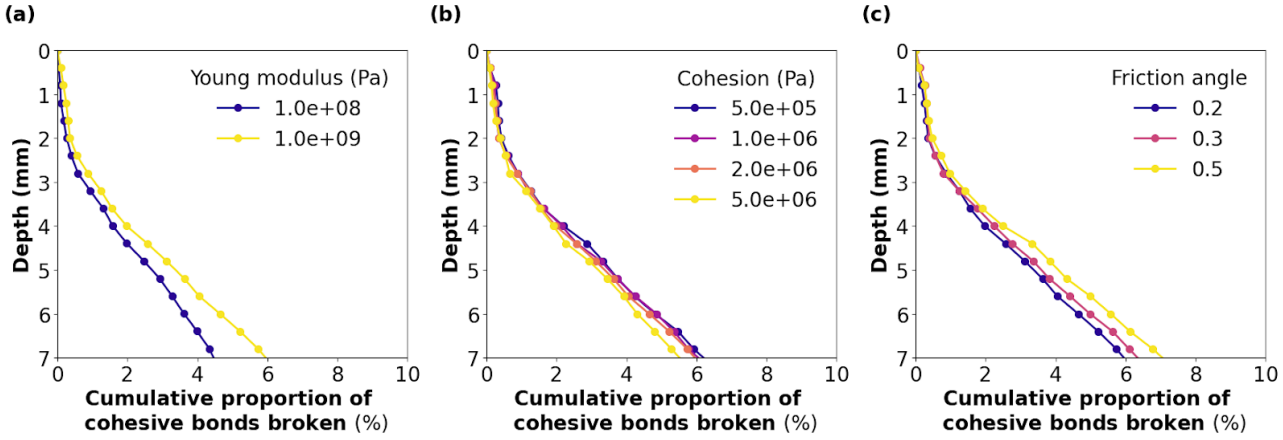

Figure S24: Influence of mechanical parameters on the cumulative number of cohesive bonds as function of tip penetration depth obtained with DEM numerical simulations of CPT. The sensitivity analysis has been performed on (a) Young's modulus E (Pa) (C = 2.0 x 10^6 Pa and tan(φ) = 0.2), (b) the Cohesion C (Pa) (E = 1.0 x 10^9 Pa and tan(φ) = 0.2) and (c) the Friction angle tan(φ) (E = 1.0 x 10^9 Pa and C = 2.0 x 10^6 Pa).

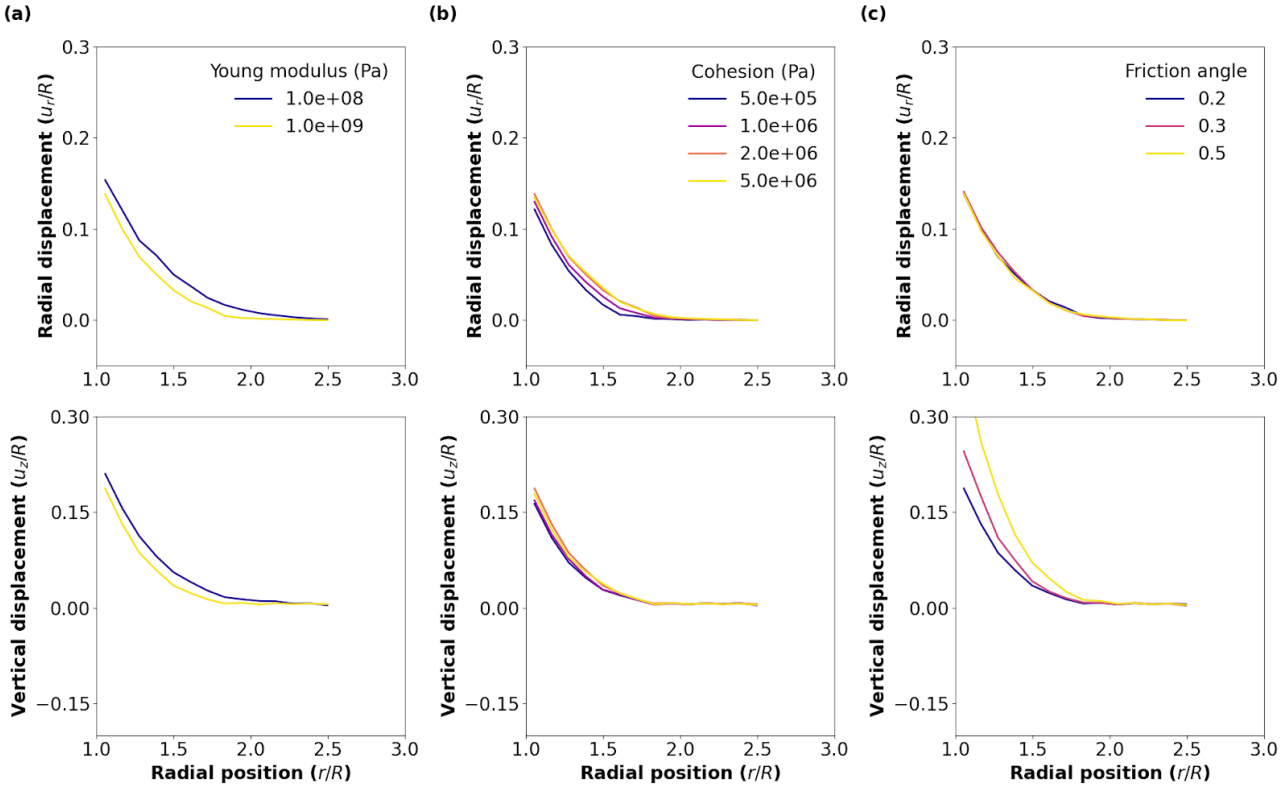

Figure S25: Influence of mechanical parameters on the vertical (top) and radial (bottom) displacement profile obtained with DEM numerical simulations of CPT. The sensitivity analysis has been performed on (a) Young's modulus E (Pa) (C = 2.0 x 10^6 Pa and tan(φ) = 0.2), (b) the Cohesion C (Pa) (E = 1.0 x 10^9 Pa and tan(φ) = 0.2) and (c) the Friction angle tan(φ) (E = 1.0 x 10^9 Pa and C = 2.0 x 10^6 Pa).

S2.3 Comparison of DEM model with experimental measurements

	E (Pa)	C (Pa)	tan(φ)	Error F (N)	Error σ (N)	Error l (mm)	Total error
RG	1 x 10^8	5 x 10^5	0.2	-8.9 x 10^{-1}	-6.3 x 10^{-1}	-1.0 x 10^{-1}	1.7 x 10^0
	1 x 10^8	5 x 10^5	0.3	-8.6 x 10^{-1}	-5.5 x 10^{-1}	-1.0 x 10^0	1.7 x 10^0
	1 x 10^8	5 x 10^5	0.5	-8.6 x 10^{-1}	-5.2 x 10^{-1}	-1.0 x 10^0	1.7 x 10^0
	1 x 10^8	1 x 10^6	0.2	-7.1 x 10^{-1}	-4.6 x 10^{-1}	-9.9 x 10^{-1}	1.5 x 10^0
	1 x 10^8	1 x 10^6	0.3	-6.5 x 10^{-1}	-4.1 x 10^{-1}	-9.9 x 10^{-1}	1.4 x 10^0
	1 x 10^8	1 x 10^6	0.5	-5.8 x 10^{-1}	-2.7 x 10^{-1}	-9.8 x 10^{-1}	1.3 x 10^0
	1 x 10^8	2 x 10^6	0.2	-1.9 x 10^{-1}	-1.9 x 10^{-1}	-9.7 x 10^{-1}	1.0 x 10^0
	1 x 10^8	2 x 10^6	0.3	5.3 x 10^{-3}	-1.1 x 10^{-1}	-9.7 x 10^{-1}	9.7 x 10^{-1}
	1 x 10^8	2 x 10^6	0.5	1.4 x 10^{-1}	8.2 x 10^{-2}	-9.3 x 10^{-1}	9.6 x 10^{-1}
	1 x 10^8	5 x 10^6	0.2	1.6 x 10^0	1.5 x 10^{-1}	-8.6 x 10^{-1}	2.4 x 10^0
	1 x 10^8	5 x 10^6	0.3	2.2 x 10^0	3.1 x 10^{-1}	-8.0 x 10^{-1}	3.2 x 10^0
	1 x 10^8	5 x 10^6	0.5	2.9 x 10^0	4.6 x 10^{-1}	-6.9 x 10^{-1}	4.3 x 10^0

	1×10^{9}	5×10^{5}	0.2	-9.6×10^{-1}	-7.0×10^{-1}	-1.0×10^{0}	1.8×10^{0}
	1×10^{9}	5×10^{5}	0.3	-9.5×10^{-1}	-6.3×10^{-1}	-1.0×10^{0}	1.8×10^{0}
	1×10^{9}	5×10^{5}	0.5	-9.4×10^{-1}	-6.0×10^{-1}	-1.0×10^{0}	1.8×10^{0}
	1×10^{9}	1×10^{6}	0.2	-9.0×10^{-1}	-4.9×10^{-1}	-9.9×10^{-1}	1.7×10^{0}
	1×10^{9}	1×10^{6}	0.3	-9.0×10^{-1}	-4.2×10^{-1}	-9.9×10^{-1}	1.7×10^{0}
	1×10^{9}	1×10^{6}	0.5	-8.7×10^{-1}	-3.0×10^{-1}	-9.8×10^{-1}	1.6×10^{0}
	1×10^{9}	2×10^{6}	0.2	-7.7×10^{-1}	-2.0×10^{-1}	-9.7×10^{-1}	1.5×10^{0}
	1×10^{9}	2×10^{6}	0.3	-7.0×10^{-1}	2.5×10^{-2}	-9.6×10^{-1}	1.4×10^{0}
	1×10^{9}	2×10^{6}	0.5	-6.8×10^{-1}	-5.9×10^{-2}	-9.4×10^{-1}	1.3×10^{0}
	1×10^{9}	5×10^{6}	0.2	-5.0×10^{-2}	3.2×10^{-1}	-8.0×10^{-1}	8.6×10^{-1}
	1×10^{9}	5×10^{6}	0.3	1.7×10^{-1}	6.4×10^{-1}	-6.8×10^{-1}	9.6×10^{-1}
	1×10^{9}	5×10^{6}	0.5	3.1×10^{-1}	5.7×10^{-1}	-5.6×10^{-1}	9.2×10^{-1}
	1×10^{10}	5×10^{5}	0.2	-9.9×10^{-1}	-8.3×10^{-1}	-1.0×10^{0}	1.9×10^{0}
	1×10^{10}	1×10^{6}	0.2	-9.6×10^{-1}	-6.7×10^{-1}	-9.9×10^{-1}	1.8×10^{0}
	1×10^{10}	2×10^{6}	0.2	-9.1×10^{-1}	-4.0×10^{-1}	-9.8×10^{-1}	1.7×10^{0}
	1×10^{10}	2×10^{6}	0.5	-8.6×10^{-1}	-3.2×10^{-1}	-9.4×10^{-1}	1.6×10^{0}
	1×10^{10}	5×10^{6}	0.2	-7.0×10^{-1}	2.6×10^{-1}	-8.0×10^{-1}	1.3×10^{0}
	1×10^{10}	5×10^{6}	0.5	-5.8×10^{-1}	5.7×10^{-1}	-5.4×10^{-1}	1.1×10^{0}
RGlr	1×10^{8}	5×10^{5}	0.2	-4.6×10^{-1}	-6.9×10^{-1}	-9.8×10^{-1}	1.4×10^{0}
	1×10^{8}	5×10^{5}	0.3	-9.1×10^{-2}	-6.7×10^{-1}	-9.8×10^{-1}	1.2×10^{0}
	1×10^{8}	5×10^{5}	0.5	7.2×10^{-1}	-4.8×10^{-1}	-9.5×10^{-1}	1.5×10^{0}
	1×10^{8}	1×10^{6}	0.2	3.5×10^{-1}	-6.2×10^{-1}	-9.6×10^{-1}	1.2×10^{0}
	1×10^{8}	1×10^{6}	0.3	1.5×10^{0}	-5.3×10^{-1}	-8.8×10^{-1}	2.4×10^{0}
	1×10^{8}	1×10^{6}	0.5	4.0×10^{0}	-2.3×10^{-1}	-8.0×10^{-1}	5.7×10^{0}
	1×10^{8}	2×10^{6}	0.2	2.7×10^{0}	-4.7×10^{-1}	-8.4×10^{-1}	4.0×10^{0}
	1×10^{8}	2×10^{6}	0.3	5.5×10^{0}	-2.5×10^{-1}	-6.6×10^{-1}	7.8×10^{0}
	1×10^{8}	2×10^{6}	0.5	1.4×10^{1}	-1.2×10^{-1}	2.6×10^{-1}	2.0×10^{1}
	1×10^{8}	5×10^{6}	0.2	1.1×10^{1}	-2.6×10^{-1}	-3.0×10^{-2}	1.5×10^{1}
	1×10^{8}	5×10^{6}	0.3	2.0×10^{1}	-9.6×10^{-2}	1.3×10^{0}	2.9×10^{1}
	1×10^{8}	5×10^{6}	0.5	4.5×10^{1}	1.4×10^{-1}	4.0×10^{0}	6.3×10^{1}
	1×10^{9}	5×10^{5}	0.2	-7.6×10^{-1}	-7.7×10^{-1}	-9.7×10^{-1}	1.6×10^{0}
	1×10^{9}	5×10^{5}	0.3	-6.2×10^{-1}	-6.9×10^{-1}	-9.3×10^{-1}	1.4×10^{0}
	1×10^{9}	5×10^{5}	0.5	-3.9×10^{-1}	-5.6×10^{-1}	-8.3×10^{-1}	1.1×10^{0}
	1×10^{9}	1×10^{6}	0.2	-4.3×10^{-1}	-6.2×10^{-1}	-8.8×10^{-1}	1.2×10^{0}
	1×10^{9}	1×10^{6}	0.3	1.7×10^{-2}	-5.1×10^{-1}	-7.2×10^{-1}	8.8×10^{-1}
	1×10^{9}	1×10^{6}	0.5	4.3×10^{-1}	-2.9×10^{-1}	-3.9×10^{-1}	7.8×10^{-1}
	1×10^{9}	2×10^{6}	0.2	4.7×10^{-1}	-3.9×10^{-1}	-4.7×10^{-1}	9.1×10^{-1}
	1×10^{9}	2×10^{6}	0.3	1.2×10^{0}	-2.4×10^{-1}	-8.9×10^{-2}	1.8×10^{0}
	1×10^{9}	2×10^{6}	0.5	2.5×10^{0}	1.1×10^{-1}	1.5×10^{0}	3.8×10^{0}
	1×10^{9}	5×10^{6}	0.2	3.7×10^{0}	-6.7×10^{-2}	1.7×10^{0}	5.5×10^{0}
	1×10^{9}	5×10^{6}	0.3	7.3×10^{0}	1.5×10^{-1}	4.2×10^{0}	1.1×10^{1}

	1×10^{9}	5×10^{6}	0.5	1.4×10^{1}	1.2×10^{0}	1.1×10^{1}	2.2×10^{1}
	1×10^{10}	5×10^{5}	0.2	-9.1×10^{-1}	-9.0×10^{-1}	-1.0×10^{0}	1.9×10^{0}
	1×10^{10}	5×10^{5}	0.3	-8.4×10^{-1}	-8.6×10^{-1}	-9.8×10^{-1}	1.8×10^{0}
	1×10^{10}	5×10^{5}	0.5	-7.3×10^{-1}	-7.4×10^{-1}	-8.8×10^{-1}	1.5×10^{0}
	1×10^{10}	1×10^{6}	0.2	-7.3×10^{-1}	-7.9×10^{-1}	-9.2×10^{-1}	1.6×10^{0}
	1×10^{10}	1×10^{6}	0.3	-5.7×10^{-1}	-6.9×10^{-1}	-7.8×10^{-1}	1.3×10^{0}
	1×10^{10}	1×10^{6}	0.5	-2.8×10^{-1}	-6.0×10^{-1}	-8.6×10^{-2}	7.2×10^{-1}
	1×10^{10}	2×10^{6}	0.2	-2.9×10^{-1}	-5.5×10^{-1}	-1.2×10^{-1}	7.0×10^{-1}
	1×10^{10}	2×10^{6}	0.3	1.3×10^{-1}	-4.3×10^{-1}	1.2×10^{0}	1.3×10^{0}
	1×10^{10}	2×10^{6}	0.5	7.3×10^{-1}	-1.9×10^{-1}	6.3×10^{0}	6.4×10^{0}
	1×10^{10}	5×10^{6}	0.2	1.2×10^{0}	-1.2×10^{-1}	6.1×10^{0}	6.3×10^{0}
	1×10^{10}	5×10^{6}	0.3	2.2×10^{0}	7.8×10^{-2}	1.3×10^{1}	1.4×10^{1}
	1×10^{10}	5×10^{6}	0.5	3.5×10^{0}	7.6×10^{-1}	3.7×10^{1}	3.7×10^{1}
DH	1×10^{8}	5×10^{5}	0.2	-6.6×10^{-1}	-7.1×10^{-1}	-9.9×10^{-1}	1.5×10^{0}
	1×10^{8}	5×10^{5}	0.5	-3.2×10^{-1}	-6.3×10^{-1}	-9.6×10^{-1}	1.2×10^{0}
	1×10^{8}	1×10^{6}	0.2	-1.7×10^{-1}	-5.5×10^{-1}	-9.6×10^{-1}	1.1×10^{0}
	1×10^{8}	1×10^{6}	0.3	3.2×10^{-1}	-4.6×10^{-1}	-9.3×10^{-1}	1.1×10^{0}
	1×10^{8}	1×10^{6}	0.5	8.3×10^{-1}	-2.4×10^{-1}	-8.8×10^{-1}	1.5×10^{0}
	1×10^{8}	2×10^{6}	0.2	1.4×10^{0}	-3.7×10^{-1}	-8.8×10^{-1}	2.2×10^{0}
	1×10^{8}	2×10^{6}	0.3	2.5×10^{0}	-3.6×10^{-1}	-7.7×10^{-1}	3.6×10^{0}
	1×10^{8}	2×10^{6}	0.5	4.8×10^{0}	6.0×10^{-2}	-4.0×10^{-1}	6.8×10^{0}
	1×10^{8}	5×10^{6}	0.2	7.1×10^{0}	-2.7×10^{-1}	-1.7×10^{-1}	1.0×10^{1}
	1×10^{8}	5×10^{6}	0.5	1.9×10^{1}	6.2×10^{-1}	2.1×10^{0}	2.7×10^{1}
	1×10^{9}	5×10^{5}	0.2	-8.5×10^{-1}	-7.6×10^{-1}	-9.8×10^{-1}	1.7×10^{0}
	1×10^{9}	5×10^{5}	0.3	5.4×10^{0}	4.0×10^{-1}	3.7×10^{0}	8.5×10^{0}
	1×10^{9}	1×10^{6}	0.2	-6.2×10^{-1}	-6.6×10^{-1}	-9.4×10^{-1}	1.5×10^{0}
	1×10^{9}	1×10^{6}	0.3	-5.1×10^{-1}	-5.6×10^{-1}	-9.0×10^{-1}	1.3×10^{0}
	1×10^{9}	1×10^{6}	0.5	-3.4×10^{-1}	-4.3×10^{-1}	-8.1×10^{-1}	1.0×10^{0}
	1×10^{9}	2×10^{6}	0.2	-1.2×10^{-1}	-4.2×10^{-1}	-8.1×10^{-1}	9.3×10^{-1}
	1×10^{9}	2×10^{6}	0.3	2.0×10^{-1}	-3.3×10^{-1}	-6.7×10^{-1}	8.0×10^{-1}
	1×10^{9}	2×10^{6}	0.5	7.2×10^{-1}	-1.4×10^{-1}	-2.3×10^{-1}	1.1×10^{0}
	1×10^{9}	5×10^{6}	0.2	2.2×10^{0}	-7.2×10^{-2}	3.3×10^{-1}	3.2×10^{0}
	1×10^{9}	5×10^{6}	0.3	-8.0×10^{-1}	-7.2×10^{-1}	-9.7×10^{-1}	1.7×10^{0}
	1×10^{9}	5×10^{6}	0.5	-7.2×10^{-1}	-6.9×10^{-1}	-9.3×10^{-1}	1.5×10^{0}
	1×10^{10}	2×10^{6}	0.2	-5.9×10^{-1}	-6.3×10^{-1}	-8.2×10^{-1}	1.3×10^{0}
	1×10^{10}	5×10^{6}	0.2	2.3×10^{-1}	-2.4×10^{-1}	7.7×10^{-1}	8.7×10^{-1}
PP	1×10^{8}	5×10^{5}	0.2	-8.1×10^{-1}	-6.7×10^{-1}	-1.0×10^{0}	1.7×10^{0}
	1×10^{8}	5×10^{5}	0.5	-7.7×10^{-1}	-6.8×10^{-1}	-1.0×10^{0}	1.6×10^{0}
	1×10^{8}	1×10^{6}	0.2	-5.4×10^{-1}	-5.8×10^{-1}	-1.0×10^{0}	1.4×10^{0}
	1×10^{8}	1×10^{6}	0.3	-4.6×10^{-1}	-6.1×10^{-1}	-1.0×10^{0}	1.3×10^{0}
	1×10^{8}	1×10^{6}	0.5	-4.1×10^{-1}	-5.3×10^{-1}	-1.0×10^{0}	1.3×10^{0}

	1×10^{8}	2×10^{6}	0.2	4.5×10^{-2}	-3.9×10^{-1}	-1.0×10^{0}	1.1×10^{0}
	1×10^{8}	2×10^{6}	0.3	2.2×10^{-1}	-4.1×10^{-1}	-9.9×10^{-1}	1.1×10^{0}
	1×10^{8}	2×10^{6}	0.5	4.1×10^{-1}	-3.6×10^{1}	-9.9×10^{-1}	1.2×10^{0}
	1×10^{8}	5×10^{6}	0.2	1.8×10^{0}	-1.7×10^{-1}	-9.8×10^{-1}	2.7×10^{0}
	1×10^{8}	5×10^{6}	0.5	2.8×10^{0}	-2.1×10^{-1}	-9.5×10^{-1}	4.0×10^{0}
	1×10^{9}	5×10^{5}	0.2	-9.3×10^{-1}	-7.6×10^{-1}	-1.0×10^{0}	1.8×10^{0}
	1×10^{9}	1×10^{6}	0.2	-8.2×10^{-1}	-5.9×10^{-1}	-1.0×10^{0}	1.6×10^{0}
	1×10^{9}	1×10^{6}	0.3	-7.9×10^{-1}	-6.0×10^{-1}	-1.0×10^{0}	1.6×10^{0}
	1×10^{9}	1×10^{6}	0.5	-7.7×10^{-1}	-5.5×10^{-1}	-1.0×10^{0}	1.6×10^{0}
	1×10^{9}	2×10^{6}	0.2	-5.3×10^{-1}	-4.3×10^{-1}	-9.9×10^{-1}	1.3×10^{0}
	1×10^{9}	2×10^{6}	0.3	-4.4×10^{-1}	-3.6×10^{-1}	-9.9×10^{-1}	1.2×10^{0}
	1×10^{9}	2×10^{6}	0.5	-4.2×10^{-1}	-3.6×10^{-1}	-9.9×10^{-1}	1.2×10^{0}
	1×10^{9}	5×10^{6}	0.2	7.6×10^{-1}	6.0×10^{-3}	-9.6×10^{-1}	1.4×10^{0}

Table S2: Combinations of all the mechanical parameters (Young's modulus E, cohesion C and friction angle tan(φ)) tested for RG, RGlr, DH and PP samples. The errors on the statistical indicators (mean force F, standard deviation , correlation length l) have been computed as relative error compared to the experimental value. Negative error value indicates an underestimation and positive error value indicates an overestimation. The total error is calculated as Total error = n error2 with n, a weight factor. The value of n is 2, 1 and 1 for $error_F$, $error_\sigma$ and $error_l$ respectively.

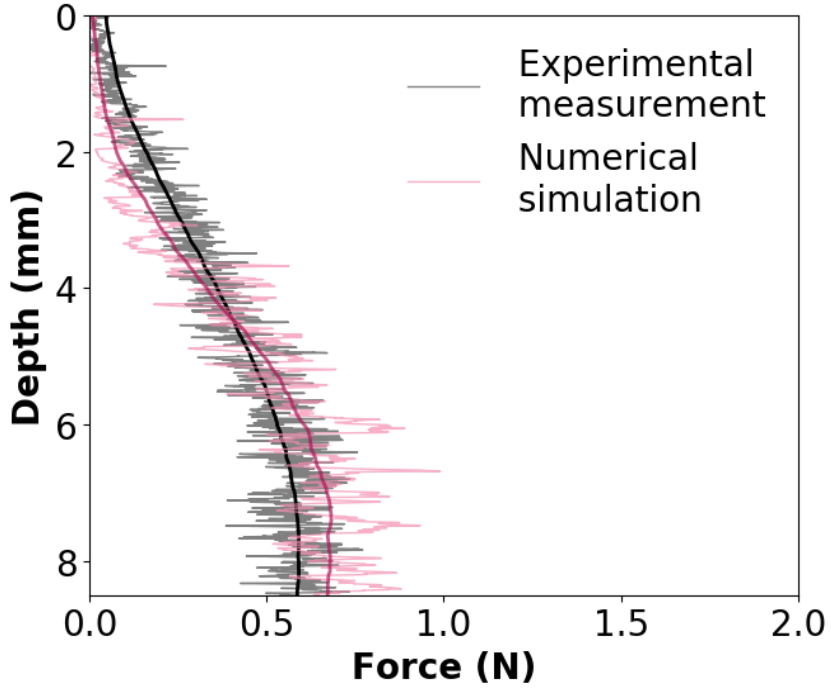

Figure S26: Experimental (grey) and numerical (coloured) force profiles obtained by CPT for RG sample. The numerical profiles correspond to the best fit of mechanical parameters (Table 3). The superposed smoothed profile (bold line) corresponds to the average force value over a rolling window of 3 mm.

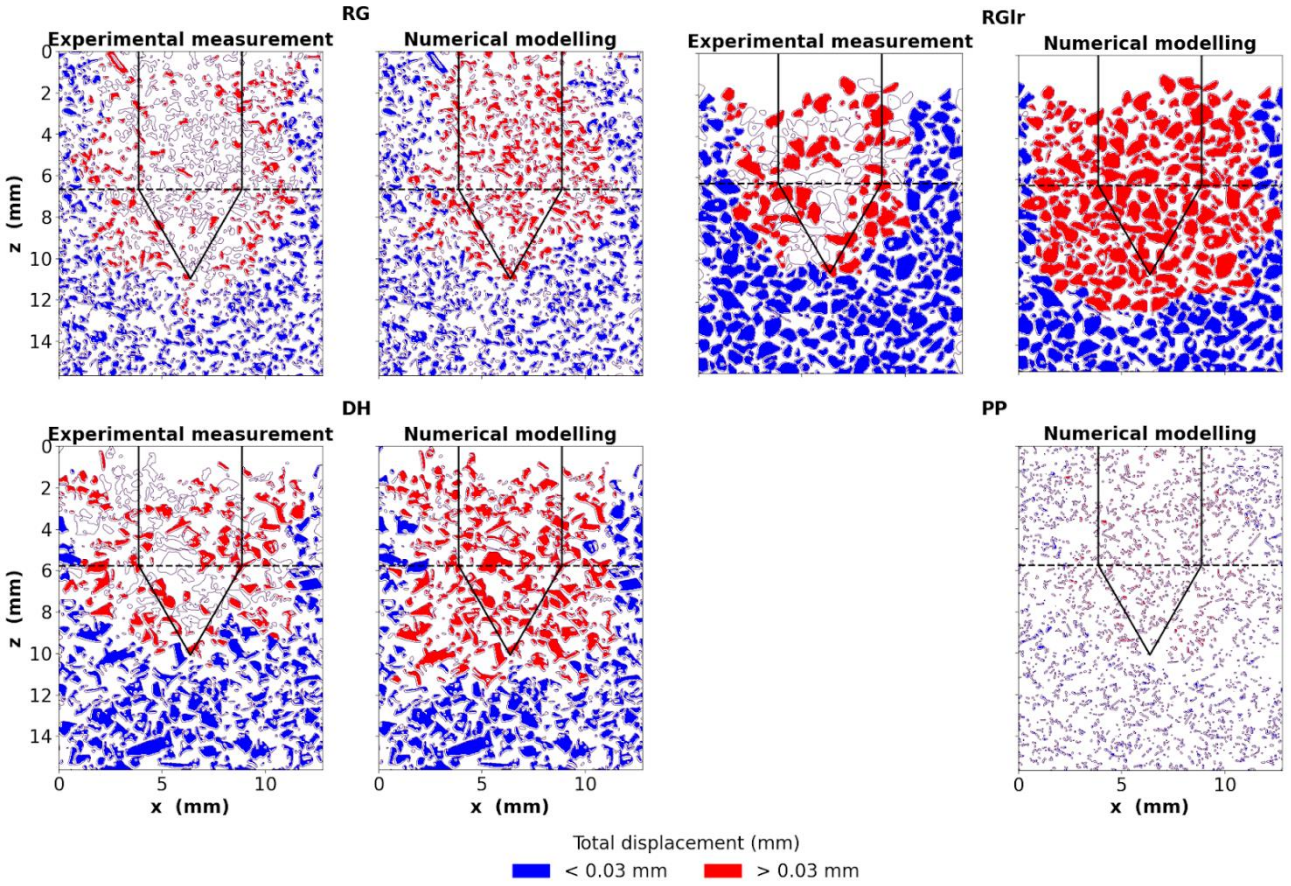

Figure S27: Total displacement maps obtained experimentally with µCT (left) and numerically with DEM simulation (right) for RG, RGlr, DH and PP samples. A displacement threshold at 0.03 mm has been set to define the deformation zone (Peinke et al. 2020). No coloured filled grains correspond to non-trackable grains in µCT scans (Peinke et al. 2020) and deleted grains in the DEM grain shape representation. The tip position is indicated with black solid lines. The horizontal black dashed line indicates the cone top. The displacement profiles are computed from the sample surface to the cone top. Results are obtained with the mechanical parameters $E = 1 \times 10^9$ Pa, $C = 2 \times 10^6$ Pa and $\tan(\varphi) = 0.2$ (Table S2).